



An unbiased high-throughput drug screen reveals a potential therapeutic vulnerability in the most lethal molecular subtype of pancreatic cancer

Chun-Hao Pan^{1,2} , Yuka Otsuka³, BanuPriya Sridharan⁴, Melissa Woo^{1,5}, Cindy V. Leiton¹, Sruthi Babu^{1,6}, Mariana Torrente Gonçalves¹, Ryan R. Kawalerski¹, Ji Dong K. Bai¹, David K. Chang^{7,8}, Andrew V. Biankin^{7,8}, Louis Scampavia³, Timothy Spicer³, Luisa F. Escobar-Hoyos^{1,9,10,11} and Kenneth R. Shroyer¹ 

1 Department of Pathology, Renaissance School of Medicine, Stony Brook University, NY, USA

2 Molecular and Cellular Biology Graduate Program, Stony Brook University, NY, USA

3 The Scripps Research Institute, Jupiter, FL, USA

4 In vitro In vivo Translation, GSK, Collegeville, PA, USA

5 Simons Summer Research Program, Stony Brook University, NY, USA

6 Department of Family, Population & Preventive Medicine, Renaissance School of Medicine, Stony Brook University, NY, USA

7 Wolfson Wohl Cancer Research Centre, Institute of Cancer Sciences, University of Glasgow, UK

8 West of Scotland Pancreatic Unit, Glasgow Royal Infirmary, UK

9 Department of Therapeutic Radiology, School of Medicine, Yale University, New Haven, CT, USA

10 David M. Rubenstein Center for Pancreatic Cancer Research, Memorial Sloan Kettering Cancer Center, New York, NY, USA

11 Genetic Toxicology and Cytogenetics Research Group, Department of Biology, School of Natural Sciences and Education, Universidad del Cauca, Popayán, Colombia

Keywords

chemoresistance; combined therapy; drug screen; keratin 17; pancreatic ductal adenocarcinoma; predictive biomarker

Correspondence

L. Scampavia, T. Spicer, The Scripps Research Institute, Florida Campus, 130 Scripps Way, Jupiter, FL 33458, USA
Tel: +1 561-228-2101 (LS); 561-228-2150 (TS)

E-mail: scamp1@scripps.edu (LS);
spicert@scripps.edu (TS)

L. F. Escobar-Hoyos, Department of Therapeutic Radiology, School of Medicine, Yale University, Hunter Building 15 York Street, Ste HRT 313B, New Haven, CT 06510, USA

Tel: +1 203-785-2956

E-mail: luisa.escobar-hoyos@yale.edu

K. R. Shroyer, Department of Pathology, Renaissance School of Medicine, Stony Brook University, 101 Nicolls Road, Stony Brook, NY 11794, USA

Tel: +1 631-444-3000

E-mail:

Pancreatic ductal adenocarcinoma (PDAC) is predicted to become the second leading cause of cancer-related deaths in the United States by 2020, due in part to innate resistance to widely used chemotherapeutic agents and limited knowledge about key molecular factors that drive tumor aggression. We previously reported a novel negative prognostic biomarker, keratin 17 (K17), whose overexpression in cancer results in shortened patient survival. In this study, we aimed to determine the predictive value of K17 and explore the therapeutic vulnerability in K17-expressing PDAC, using an unbiased high-throughput drug screen. Patient-derived data analysis showed that K17 expression correlates with resistance to gemcitabine (Gem). In multiple *in vitro* and *in vivo* models of PDAC, spanning human and murine PDAC cells, and orthotopic xenografts, we determined that the expression of K17 results in a more than twofold increase in resistance to Gem and 5-fluorouracil, key components of current standard-of-care chemotherapeutic regimens. Furthermore, through an unbiased drug screen, we discovered that podophyllotoxin (PPT), a microtubule inhibitor, showed significantly higher sensitivity in K17-positive compared to K17-negative PDAC cell lines and animal models. In the clinic, another microtubule inhibitor, paclitaxel (PTX), is used in combination with Gem as a first-line chemotherapeutic regimen for PDAC. Surprisingly, we found that when combined with Gem, PPT, but not PTX, was synergistic in inhibiting the viability of K17-expressing PDAC cells. Importantly, in preclinical

Abbreviations

5-FU, 5-fluorouracil; APGI, Australian Pancreatic Cancer Genome Initiative; CI, combination index; FDA, U.S. Food and Drug Administration; Gem, gemcitabine; K17, keratin 17; LOPAC, Library of Pharmacologically Active Compounds; PDAC, pancreatic ductal adenocarcinoma; PPT, podophyllotoxin; PTX, paclitaxel.

kenneth.shroyer@stonybrookmedicine.edu

Chun-Hao Pan and Yuka Otsuka contributed equally to this work.

(Received 7 October 2019, revised 26 March 2020, accepted 3 June 2020, available online 4 July 2020)

doi:10.1002/1878-0261.12743

models, PPT in combination with Gem effectively decreased tumor growth and enhanced the survival of mice bearing K17-expressing tumors. This provides evidence that PPT and its derivatives could potentially be combined with Gem to enhance treatment efficacy for the ~ 50% of PDACs that express high levels of K17. In summary, we reported that K17 is a novel target for developing a biomarker-based personalized treatment for PDAC.

1. Introduction

Pancreatic ductal adenocarcinoma (PDAC) is one of the deadliest cancers, with a 5-year survival rate at only 7% [1]. This extremely poor prognosis is due in part to the lack of effective screening strategies to detect PDAC at early stages [2] and to the inherent resistance of these tumors to currently available first-line chemotherapeutic agents [3,4].

The majority of patients are diagnosed at late metastatic or advanced stages, and as a result, only 10–15% of PDACs are candidates for surgical resection [5]. With or without surgery, patients are subjected to chemotherapy where gemcitabine (Gem) was the baseline treatment for more than a decade and is still employed [6]. Currently, Gem combined with paclitaxel albumin-bound nanoparticles (nab-PTX, Abraxane) [7] and the FOLFIRINOX regimen [5-fluorouracil (5-FU), leucovorin, irinotecan, and oxaliplatin] [8] are two standard-of-care therapies that have been found to improve the survival rates compared to the use of Gem alone [9]. However, despite this improvement, PDACs usually show only weak response to all current treatment regimens [10]. Therefore, exploring biomarker-driven novel therapies is a critical priority for improving therapeutic outcomes for PDAC patients.

To this end, it was reported and recently validated in several cohorts that PDAC is composed of molecular subtypes, based on distinct gene expression profiles that impact on patient survival [11–14]. These differential gene expression signatures are now being used as biomarkers for molecular subtyping [15–17], however, whether the proteins encoded by these genes cause resistance to treatment and whether they could be exploited as therapeutic targets for PDAC remain unexplored.

We independently demonstrated that keratin 17 (K17), one signature gene overexpressed in the basal-like PDAC [14], is an independent negative prognostic biomarker and is as accurate as molecular subtyping

to predict PDAC patient survival [17]. However, it is still unknown if K17 is predictive for treatment response and if K17 expression in PDAC cells sensitizes them to specific and currently available small-molecule inhibitors. To address these questions, we evaluated K17 mRNA expression of PDACs from patients that received Gem treatment as standard-of-care vs no treatment. This led us to identify that K17 is a predictive marker of Gem response. In addition, a high-throughput small-compound screen uncovered a novel therapeutic vulnerability of tumors bearing K17 expression. Our findings support the conclusion that K17 could be a target for the development of a novel, and potentially more effective biomarker-based personalized therapy for PDAC.

2. Materials and Methods

2.1. Prognostic and predictive value analyses from patient-derived samples

K17 mRNA expression levels of PDAC cases were acquired from the Australian Pancreatic Cancer Genome Initiative (APGI) [11]. K17 mRNA expression and survival were evaluated in 94 PDAC patients that were treated with adjuvant Gem alone or received no treatment. Based on the established cutoff of the maximum-likelihood fit of a Cox proportional hazard model [17], we applied the 76th percentile of mRNA expression to categorize patients into high-K17 vs low-K17 groups. Overall survival in high- vs low-K17 mRNA was determined using the Kaplan–Meier method, calculated from the date of diagnosis to the date of death. Patients still alive at the last follow-up were censored. Prognostic and predictive analyses were performed based on the criteria described by Ballman [18]. Adjusting for potential confounders, a multivariate analysis was performed by Cox proportional hazard regression. Statistical significance was set at $P < 0.05$, and analysis was done using SAS 9.4 (SAS

Institute, Cary, NC, USA) and GRAPHPAD PRISM 7 (GraphPad software, San Diego, CA, USA).

2.2. Pharmacological and genomic analysis

CellMinerCDB, a web-based resource [19], was used to determine the correlation of K17 expression and sensitivity of Gem or 5-FU in pancreatic adenocarcinoma cell lines. In the datasets, drug sensitivity ($-\log_{10}[\text{IC}_{50}, \text{M}]$) was measured using sulforhodamine B total protein cytotoxicity assay at 48 h post-treatment, and K17 mRNA expression (z -score from microarray \log_2 intensity) was measured by Agilent Whole Human Genome Oligo Microarray (Santa Clara, CA, USA). The GDSC-MGH-Sanger dataset was used to perform the analyses. Pearson's correlation and P -value were calculated. Analyzed data are shown in Tables S1 and S2.

2.3. Compounds tested

Gem (purity > 99%), 5-FU (purity > 99%), podophylotoxin (PPT, purity > 99%), taxol (PTX, purity > 95%), mitoxantrone (purity > 99%), and tyrphostin AG 879 (purity > 99%) were purchased from Sigma-Aldrich (St. Louis, MO, USA). These drugs were dissolved in 100% DMSO (Fisher BioReagents, Pittsburgh, PA, USA) with a stock concentration of 20 mM and were prepared for cell experiments at final DMSO concentrations at 0.1%.

2.4. Cell culture

Human L3.6 PDAC cell line (Kras^{G12A}) [20] was a gift from W.-X. Zong (Rutgers University). MIA PaCa-2 PDAC cells (Kras^{G12C}, p53R^{248W}) were obtained from American Type Culture Collection (Manassas, VA, USA). Murine Kras^{G12D}, p53^{R172H} pancreatic cancer cells (KPC) cell line was a gift from G. Mackenzie (University of California at San Diego). Cells were cultured at 37 °C in a humidified incubator under 5% CO₂ in Dulbecco's modified Eagle's medium (DMEM; Gibco, Waltham, MA USA) supplemented with 10% FBS (Thermo Fisher, Waltham, MA USA) and 1% penicillin and streptomycin (P/S, Gibco).

2.5. CRISPR-Cas9-mediated K17 knockout in PDAC cell line

CRISPR-Cas9-mediated knockout (KO) cell pool of K17 (KRT17, gene name) in L3.6 cells was generated by Synthego Corporation (Redwood City, CA, USA). To generate these cells, ribonucleoproteins containing the Cas9 protein and the synthetic chemically modified

single-guide RNA (CCAGTACTACAGGACAATTG) were electroporated into the cells using Synthego's optimized protocol (<https://www.synthego.com/resources/all/protocols>). The genetic editing efficiency was assessed upon recovery (48 h postelectroporation). Genomic DNA was extracted from the cells, PCR-amplified, and sequenced using Sanger sequencing. The resulting chromatograms were processed using Synthego Inference of CRISPR edits software (ice.synthego.com).

2.6. Overexpression of K17 in PDAC cell lines

To generate L3.6 K17 Rescue cell line model, cells were stably transduced to express either empty vector (EV) or human K17 (K17 Rescue). In brief, cells were transduced in medium supplemented with 1% FBS for 18 h, followed by puromycin antibiotic selection for 7 days. To generate K17 gain-of-function (GOF) cell line models, MIA PaCa-2 and KPC cells were stably transduced to express either EV or human K17 (K17). Briefly, cells were transduced in medium supplemented with 10% FBS for 24 h, followed by fluorescence-activated cell sorting.

2.7. Protein extraction and western blot analysis

Cells were harvested using RIPA buffer containing protease and phosphatase inhibitor cocktail (Thermo Fisher Scientific). The lysates were sonicated and centrifuged at 16 000 g for 10 min, and the supernatant was collected. The protein concentration of the cell lysates was measured using a Bradford Protein Assay Kit (Bio-Rad, Hercules, CA, USA) according to the manufacturer's instructions. Equal amounts of proteins were separated by 12% SDS/PAGE. Immunoblotting was performed with primary antibodies to K17 [21–23] (a gift from P. Coulombe, University of Michigan) and GAPDH (Cell Signaling Technology, Danvers, MA, USA), followed by infrared goat anti-mouse or goat anti-rabbit IgG secondary antibodies (LI-COR Inc., Lincoln, NB, USA). Western blot images were captured by LI-COR Odyssey Imaging machine, and images were quantified using IMAGE STUDIO LITE software (LI-COR Inc.).

2.8. Immunofluorescence imaging

Cells were first fixed in ice-cold methanol for 5 min at 20 °C, permeabilized with 0.25% Triton X-100 for 10 min at room temperature, and blocked in 10% donkey serum (Sigma-Aldrich) dissolved in PBS (Gibco) for 1 h. Primary K17 antibody [23] diluted in 10%

donkey serum was incubated overnight. Fluorescence-conjugated goat anti-rabbit secondary antibody (Abcam, Cambridge, MA, USA) was incubated at dark for 1 h. Cells were mounted with VECTA-SHIELD (Vector Laboratories, Burlingame, CA, USA) with DAPI.

2.9. Murine orthotopic xenograft studies

All experimental procedures described were approved by the Institutional Animal Care and Use Committee at Stony Brook University and are in accordance with the Guide for the Care and Use of Laboratory Animals from the National Institutes of Health. For implantation per animal, KPC cells stably expressing either EV or K17 were harvested during the log-phase growth and resuspended in DMEM (Gibco) with Matrigel (Life Sciences, Tewksbury, MA, USA) at a ratio of 1 : 1, to a final of 1000 cells in a 30 μ L volume. Cells were orthotopically implanted into the head of the pancreas of c57B6J mice. Tumor growth was measured weekly via 3D ultrasound imaging starting 11 days postimplantation using Vevo 3100 Preclinical Imaging System (FUJIFILM VisualSonics, Toronto, ON, Canada). Once the tumor volume reached around 50 mm³, the mice were randomized into treatment groups and administered the following agents through intraperitoneal injections: Study I: Gem chemoresistance study—(a) vehicle and (b) Gem alone (at a dosage of 50 mg·kg⁻¹ body weight administered twice a week. Gem was dissolved in PBS); Study II: 5-FU chemoresistance study—(a) vehicle and (b) 5-FU alone (at a dosage of 50 mg·kg⁻¹ body weight administered twice a week. 5-FU was dissolved in PBS); and Study III: Gem in combination with PPT study—(a) vehicle, (b) PPT alone (at a dosage of 4 mg·kg⁻¹ body weight administered twice a week. PPT was dissolved in PBS), and (c) combination of Gem and PPT (Gem at a dosage of 25 mg·kg⁻¹ body weight administered on the first and fourth days of the week, and PPT at a dosage of 4 mg·kg⁻¹ body weight administered on the second and fifth days of the week; preparations of each agent were the same as in the single-treatment group). Tumor growth and body weight were monitored weekly.

2.10. The Library of Pharmacologically Active Compounds drug screening

The library currently available at Scripps was purchased from Sigma-Aldrich. Two screens were performed in 1536-well format, which include a screen performed in L3.6 K17-expressing cells and

counterscreen in L3.6 K17 KO cells. Cell viability was examined using the CellTiter-Glo[®] Luminescent Cell Viability Assay (Promega, Madison, WI, USA), a homogeneous method to determine the number of viable cells in culture based on quantitation of the ATP present, which signals the presence of metabolically active cells. First, 500 cells per well in a 5 μ L volume were plated (Greiner part # 789173) in DMEM (10% FBS + 1% P/S) and incubated overnight at 37 °C in an incubator under 5% CO₂, and then, compounds were added at 2 μ M final concentration followed by an additional incubation for 48 h. Next, 5 μ L of CellTiter-Glo[®] reagent was added to all wells. After incubation at room temperature for 10 min to ensure stabilization of luminescence, the plate was read by ViewLux[™] (PerkinElmer, Waltham, MA, USA). Raw assay data were analyzed using SYMYX software (Symyx Technologies Inc., Santa Clara, CA, USA). Activity of each compound was calculated based on average +3 standard deviation using the following equation:

$$\text{Percent Response of Compound} = 100 \times \left(\frac{\text{Test Well} - \text{Median Data Wells}}{\text{Median High Control} - \text{Median Data Wells}} \right)$$

Test Well = cells + compound; Data Wells = all test wells; High Control = media only plus DMSO. A mathematical algorithm was used to determine active compounds (Hits). Two values were calculated: (a) the average percent response of all compounds and (b) three times their standard deviation. The sum of these two values was used as a cutoff parameter, that is, any compound that exhibited greater percent activation than the cutoff parameter was declared active as a hit ($P < 0.0001$).

2.11. Cell viability and proliferation assays

Cell viability was examined using the CellTiter-Glo[®] Luminescent Cell Viability Assay (Promega) or the WST-1 cell proliferation reagent (Sigma-Aldrich), using the method described previously [24]. Cells were plated in 96-well plate at 6×10^4 cells per well and incubated overnight, and drugs were added with 10-point dose–response titrations in triplicate (0.5–20 000 nM) or at indicated concentration for 48 h. For WST-1 colorimetric assay, 10 μ L of WST-1 was added per well, and the plate was incubated for 30 min and gently shaken. The absorbance was measured using a microplate (ELISA) reader at 450 nm and the reference at 630 nm. Representative dose–response curves are included in Fig. S4. To measure cell

proliferation, cells were plated at 4×10^4 cells per well in 96-well plates and the relative proliferation index was measured by WST-1 assay at each time point.

2.12. Flow cytometric cell cycle analysis

The percent cells at each cell cycle phase were assessed through propidium iodide (PI; Sigma-Aldrich) nuclear staining. Cells were seeded at 3×10^5 cells per dish in 60-mm dishes for 24 h and were exposed to DMSO or PPT treatment at 20 nM for 48 h (L3.6 and MIA PaCa-2) or 60 h (KPC). After treatments, cells were harvested and stained with PI in Kreshan modified buffer for 30 min. The percent cells at each cell cycle phase and apoptosis were measured by flow cytometry (BD Biosciences, Franklin Lakes, NJ, USA), and data were analyzed by ModFit LT™ (Verity Software House, Topsham, ME, USA).

2.13. Statistics

The half-maximal inhibitory concentration (IC₅₀) of single-drug treatment was determined by GRAPH PAD PRISM 7 (Graph Pad Software) or SYMYX software (Symyx Technologies Inc.). The specificity of compounds was calculated by specificity = (IC₅₀ of KO)/(IC₅₀ of WT) and defined as follows: < 0.5: low; between 0.5 and 2: medium; and > 2: high. The combination index (CI) and IC₅₀ for drug combinations were calculated using COMPUSYN software (www.combosyn.com), according to the Chou–Talalay model, one of the most widely used methods for detecting and quantifying synergistic interactions between drugs [25]. CI < 0.9 indicates a synergistic effect. CI = 0.9–1.2 indicates an additive effect. CI > 1.2 indicates an antagonistic effect. The statistical significance between two groups was determined using Student's *t*-test. Data were expressed as means ± standard deviation (SD) or standard error mean (SEM), and **P* < 0.05, ***P* < 0.01, and ****P* < 0.001 were considered significant.

3. Results

3.1. K17 is a novel predictive biomarker of gemcitabine chemotherapy in PDAC

We previously reported that K17 is a prognostic biomarker for PDAC patients. Here, we set out to test whether K17 could be a predictive biomarker in PDAC. Using APGI patient data [11], we first defined K17 status in PDACs by analyzing K17 mRNA

expression and applying the previously established cut-off [17] to categorize high- and low-K17 cases (K17 mRNA *Z*-scores ranged from −0.66 to 11.17). High-K17 cases were defined as those in the top 24th percentile of K17 expression, while low-K17 cases were the lowest 76th percentile (Fig. 1A). This 76th threshold, which provides maximal stratification of survival differences based on K17 mRNA expression, was trained and subsequently adjusted previously. We first validated the prognostic value of K17. Patients with high-K17 PDACs had a shorter median survival (14 months) than patients with low-K17 PDACs (23 months; HR = 1.8, log-rank *P* = 0.0334; Fig. 1B). Furthermore, the prognostic value of K17 mRNA status was independent of pathological stage (Fig. 1C).

To determine whether K17 expression predicts response to treatment with Gem, we analyzed the survival of patients harboring high- or low-K17-expressing tumors, comparing treatment of Gem alone (adjuvant Gem) or no treatment using the APGI data. The low-K17 group treated with adjuvant Gem had a median survival of 32 months, which was significantly longer than the no-treatment group, with a median survival of 9 months (HR = 0.34, log-rank *P* = 0.0002; Fig. 1D). In contrast, the high-K17 PDACs did not show differences in the median survival between adjuvant Gem and no-treatment groups (HR = 0.95, log-rank *P* = 0.9167; Fig. 1E). This showed that the low-K17 group responded to Gem treatment but high-K17 group did not show any treatment response, suggesting that there was a qualitative predictive interaction according to Ballman *et al.* [18]. Thus, beyond its role as a prognostic biomarker for PDAC, K17 is predictive for the response to Gem.

3.2. K17 actively drives chemoresistance to first-line therapeutic agents

Given an association between K17 expression and resistance to Gem, we set out to identify whether K17 expression actively promotes resistance to Gem and another key chemotherapeutic agent 5-FU, which are major components for the two first-line chemotherapies. To test this, we first analyzed the correlation of K17 mRNA expression and chemoresistance in a panel of PDAC cell lines, using CellMinerCDB, a web-based resource for integrating pharmacological and genomic analysis. We found that K17 mRNA expression was negatively correlated with sensitivity to Gem (Pearson's *r* = −0.5576, *P* = 0.0477) and 5-FU (Pearson's *r* = −0.6004, *P* = 0.0232; Fig. 2A,B), suggesting that cell lines expressing higher level of K17 were less sensitive to Gem and 5-FU. Therefore, K17 expression is

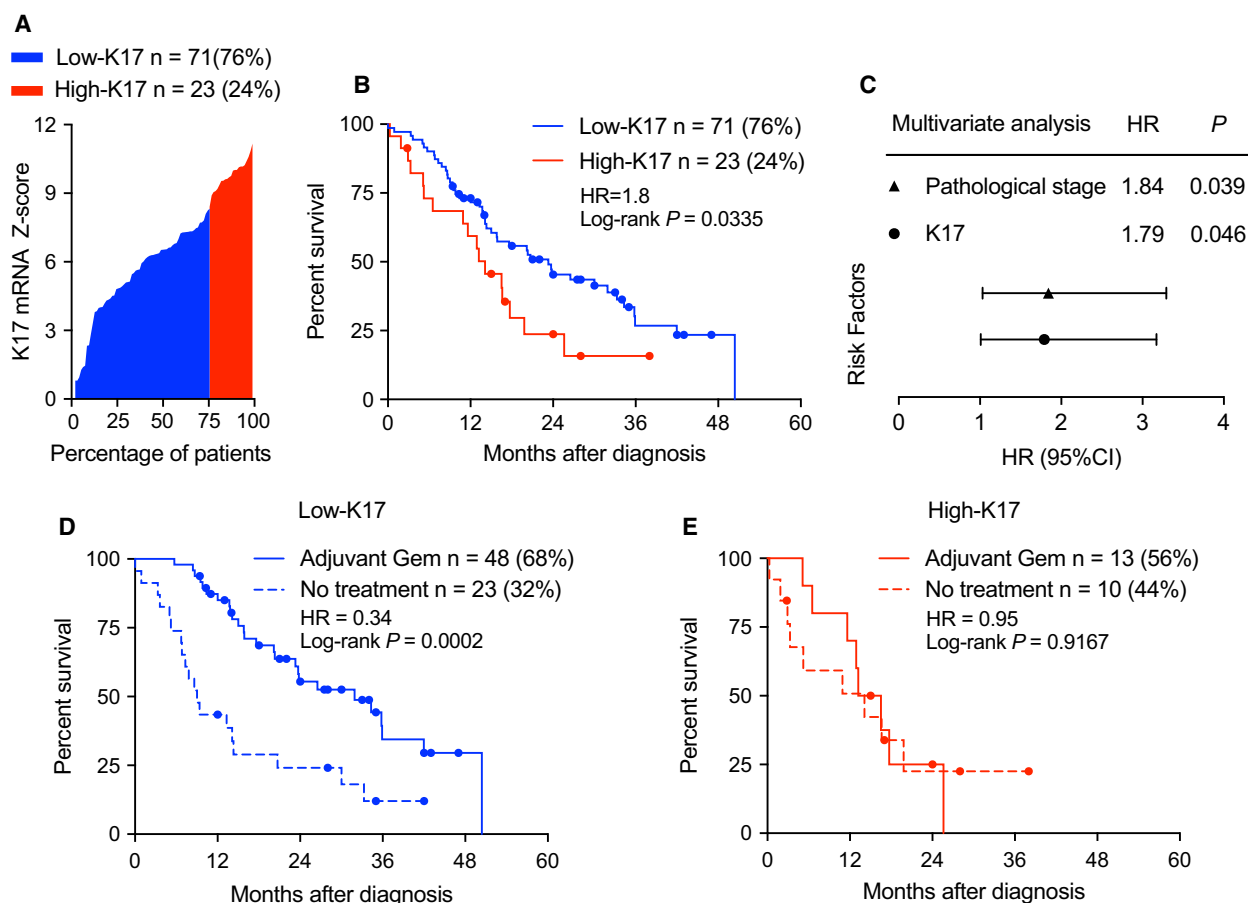


Fig. 1. K17 predicts response of Gem in PDAC patients. (A) K17 mRNA expression level of patient samples from the APGI cohort is shown in a waterfall plot. The established cutoff of 76th percentile [17] was applied to categorize patients into high- and low-K17 groups. 76% of PDAC cases below cutoff were classified as low-K17 (blue), and 24% of cases above the cutoff were defined as high-K17 (red). (B) Kaplan–Meier curves show the overall survival of patients with high-K17 and low-K17 PDACs. Hazard ratios (HR) and log-rank P -value are shown. (C) Forest plot shows the multivariate analysis from risk factors of the pathological stage and K17 mRNA as a binary variable. Pathological stage and K17 show significant P -values. (D) Patients with low-K17 PDACs exhibited significantly longer survival after adjuvant Gem therapy, compared with those who did not receive Gem. HR and log-rank P -value are shown. (E) Patients with high-K17 PDACs exhibited no overall survival differences between groups with or without Gem treatment. HR and log-rank P -value are shown.

correlated with resistance to lead chemotherapeutic agents used for PDAC standard-of-care treatment.

To test whether K17 causes chemoresistance, we next generated a K17 loss-of-function (LOF) human cell line model to assess the response to Gem and 5-FU. Using CRISPR-Cas9 technology, we knocked out endogenous expression of K17 from L3.6 human PDAC cell line (Fig. 2C,D). Isogenic cells with and without expression of K17 were treated with Gem or 5-FU, and the IC₅₀ was determined. We found that K17-expressing cells showed significantly higher IC₅₀ values of Gem (Fig. 2E, twofold) and 5-FU (Fig. 2F, twofold) compared with K17 KO cells. In addition, we performed rescue experiments to assess IC₅₀ values, using isogenic conditions with K17 KO cells that were

stably transduced to re-express K17 (K17 Rescue) or controls (EV; Fig. 2G,H). We found that K17 Rescue cells had significantly increased IC₅₀ values of Gem (Fig. 2I, 14-fold) and 5-FU (Fig. 2J, ninefold) compared with control cells (EV).

We further validated these results in K17 GOF cell line models. Human PDAC cell line MIA PaCa-2 (Fig. 2K,L) and murine Kras^{G12D}, p53^{R172H} pancreatic cancer cells (KPC Fig. 2M,N), which express low level of K17, were stably transduced to express K17 as K17 GOF cell line models. As proof of principle, K17-expressing cells showed significantly higher IC₅₀ values compared to non-K17-expressing cells after treated with Gem (Fig. 2O, MIA PaCa-2: 10-fold, KPC: fivefold) and 5-FU (Fig. 2P, MIA PaCa-2: threefold,

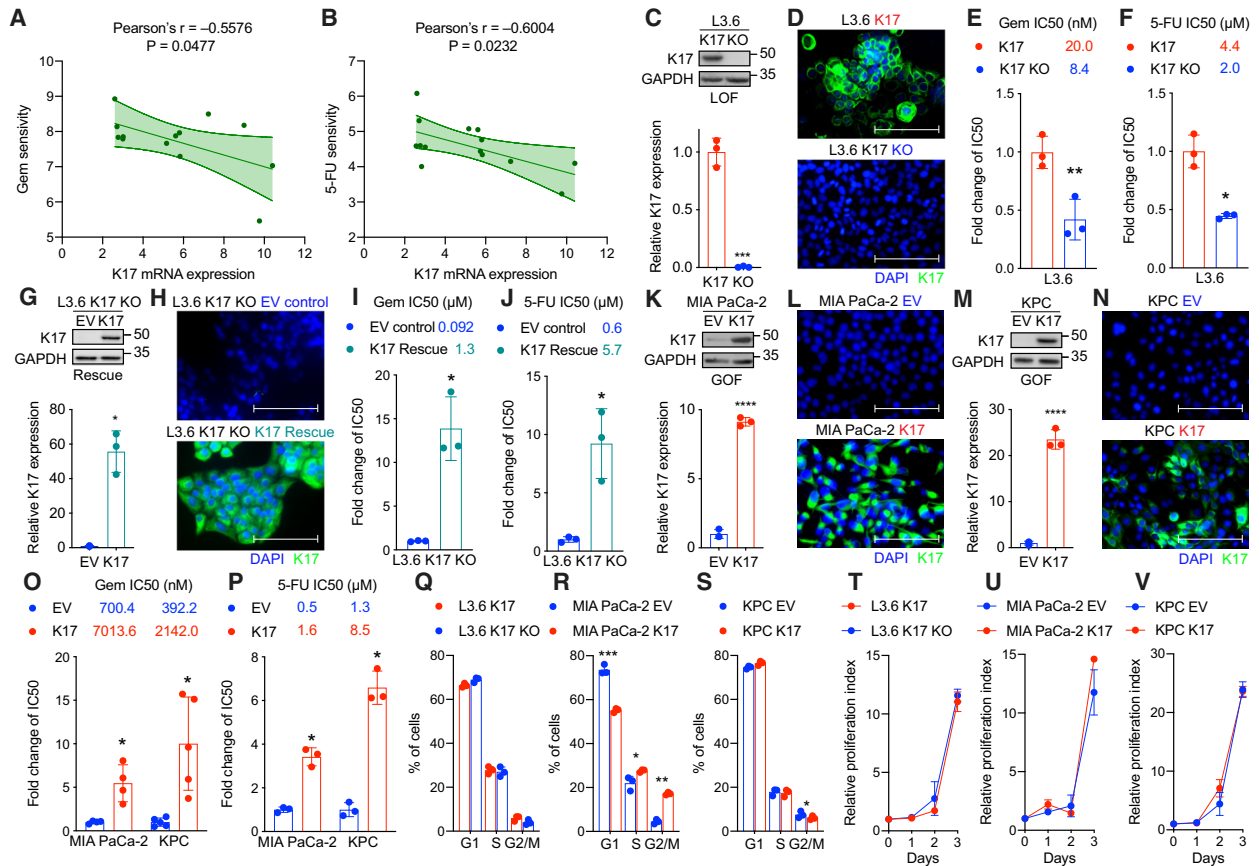


Fig. 2. K17 causes chemoresistance to Gem and 5-FU in PDAC. (A, B) There is a significantly negative correlation of K17 mRNA expression with Gem (A) and 5-FU (B) sensitivity in pancreatic adenocarcinoma cell lines. (C) Genetic manipulation of K17 expression to generate stable cell line model. K17 LOF model: L3.6 human PDAC cell line expresses endogenous K17. CRISPR-Cas9 technique was used to generate K17 KO cells. Western blot and quantification are shown. (D) Immunofluorescence images of L3.6 cell line model. Filament form of K17 is shown in green, and the nucleus is indicated by DAPI stain in blue. (E, F) L3.6 cells expressing K17 showed significantly higher IC50 value of Gem (E) and 5-FU (F) than cells had K17 KO. IC50 values and fold change of IC50 are shown. (G) Generation of K17 Rescued cell line model. L3.6 K17 KO cells were transduced to stably express either EV or human K17 (K17). Western blot and quantification are shown. (H) Immunofluorescence images of L3.6 K17 Rescued cell line model. Filament form of K17 is shown in green, and the nucleus is indicated by DAPI stain in blue. (I, J) L3.6 cells re-expressing K17 showed significantly higher IC50 values of Gem (I) and 5-FU (J) than control cells (EV). IC50 values and fold change of IC50 are shown. (K) Generation of human K17 GOF cell line model. MIA PaCa-2 PDAC cell line expresses low level of K17. Cells were transduced to stably express either EV or human K17 (K17) as a human K17 GOF model. Western blot and quantification are shown. (L) Immunofluorescence images of MIA PaCa-2 cell line model. Filament form of K17 is shown in green, and the nucleus is indicated by DAPI stain in blue. (M) Generation of murine K17 GOF cell line model. Murine Kras^{G12D}, p53^{R172H} pancreatic cancer cells (KPC) barely express K17. Cells were transduced to stably express either EV or human K17 (K17) as a K17 GOF model. Western blot and quantification are shown. (N) Immunofluorescence images of KPC cell line model. Filament form of K17 is shown in green, and the nucleus is indicated by DAPI stain in blue. (O, P) K17 causes chemoresistance to Gem (O) and 5-FU (P) in K17 GOF cell line models. K17-expressing KPC and MIA PaCa-2 cells had significantly higher IC50 values. IC50 values and fold change of IC50 are shown. (Q–S) Cell cycle analyses of K17 cell line models: L3.6 (Q), MIA PaCa-2 (R), and KPC (S). (T, V) Proliferation curves of K17 cell line models: L3.6 (T), MIA PaCa-2 (U), and KPC (V). No difference in proliferation between K17-positive and K17-negative cells was found. Data are shown in mean \pm SD. * P < 0.05, ** P < 0.01, *** P < 0.001, **** P < 0.0001, n = 3–5. Student's t -test. Scale bar = 100 μ m.

KPC: sevenfold). Importantly, we did not detect any large difference in cell cycle progression (Fig. 2Q–S) or proliferation rates (Fig. 2T–V) between K17-positive and K17-negative cells in these cell line models, suggesting that the differences in response to Gem and 5-FU are not related to differences in cell division.

To strengthen our *in vitro* findings, we employed a preclinical mouse model to determine the response of Gem and 5-FU. Mouse pancreata were orthotopically implanted with KPC cells with or without K17 expression. When tumors reached around 50 mm³, we started treatments of Gem or 5-FU. After Gem

treatment, in tumors without K17 expression (EV), the tumor size was significantly inhibited compared with saline-treated controls (Fig. 3A,B, blue bars). In contrast, in tumors expressing K17 (K17), there was no difference of tumor volume between Gem- and saline-treated groups (Fig. 3A,B, red bars). Similar results were found in mice given 5-FU treatment (Fig. 3C,D). Mice bearing K17-expressing tumors and treated with Gem or 5-FU grew 4.3 and 2.5 times larger than isogenic tumors treated with the same agents. These findings indicate that K17 expression enhances the intrinsic resistance to chemotherapeutic agents in PDAC cells in a cell-autonomous matter, suggesting that K17 could be used as a novel predictive biomarker in PDAC.

3.3. An unbiased high-throughput drug screen reveals compounds that specifically target K17-expressing PDAC

Considering that K17 expression drives chemoresistance to first-line therapeutic agents [26] and that there are currently no therapeutic agents to target this intermediate filament, we set out to screen for small molecules that preferentially impact K17-expressing PDAC cells, with the goal of identifying therapeutic

vulnerabilities in these cells and enhancing their response to current standard-of-care treatment.

We performed two high-throughput screens in isogenic L3.6 cells with or without expression of K17, against compounds from the Library of Pharmacologically Active Compounds (LOPAC) to identify the most effective and specific agents against K17-expressing cells (Fig. 4A). The primary screen yielded 24 active compounds (hits) that showed high response rates in L3.6 K17-expressing cells (Table 1). After completion of the first screen with K17-expressing cells, we performed a counterscreen assay with isogenic counterpart L3.6 K17 KO cells, and it yielded 16 active hits (Table 1). The hits from both the primary screen and counterscreen ($P < 0.0001$) were then evaluated for overlap and grouped into three categories. In these single-dose high-throughput screens, 10 compounds were found to be selective for K17-expressing cells, 14 compounds were found to equally target both K17-expressing and K17 KO cells, and 2 compounds were found to be selective for K17 KO cells (Fig. 4B, Table 1).

With the goal of targeting K17-expressing PDACs, we focused on validating the 10 identified compounds that showed higher response rates in K17-expressing cells compared with non-K17-expressing cells. These

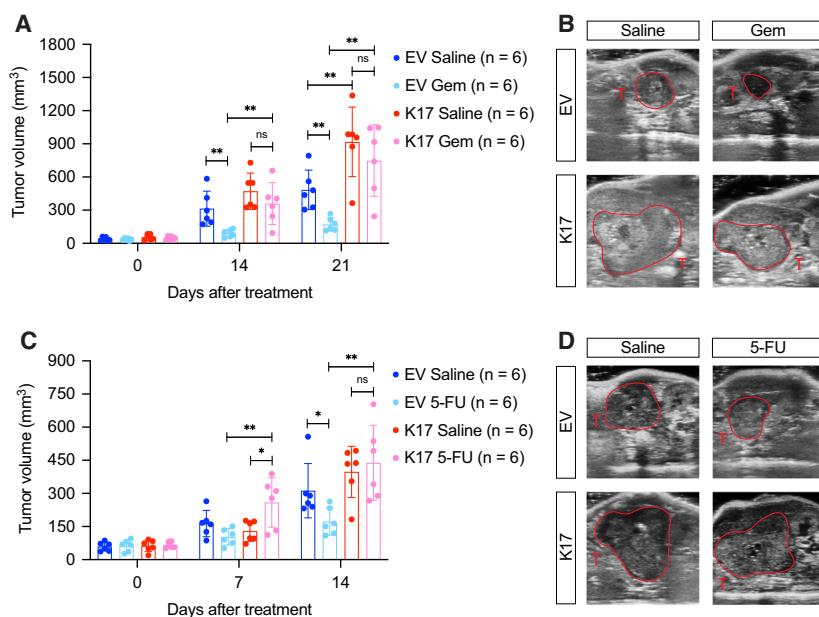


Fig. 3. Tumor volume of K17-expressing PDACs is not decreased by Gem or 5-FU treatment. (A) With Gem treatments, tumor volumes of KPC non-K17-expressing tumors (EV) were decreased while K17-expressing tumors (K17) were not decreased. (B) Representative ultrasound images of tumors with or without K17 expression from Gem treatment and control. T, tumor. (C) With 5-FU treatments, tumor volumes of KPC non-K17-expressing tumors (EV) were decreased while K17-expressing tumors (K17) were not decreased. (D) Representative ultrasound images of tumors with or without K17 expression from 5-FU treatment and control. Data are shown in mean \pm SD. * $P < 0.05$, ** $P < 0.01$, $n = 6$. Student's *t*-test.

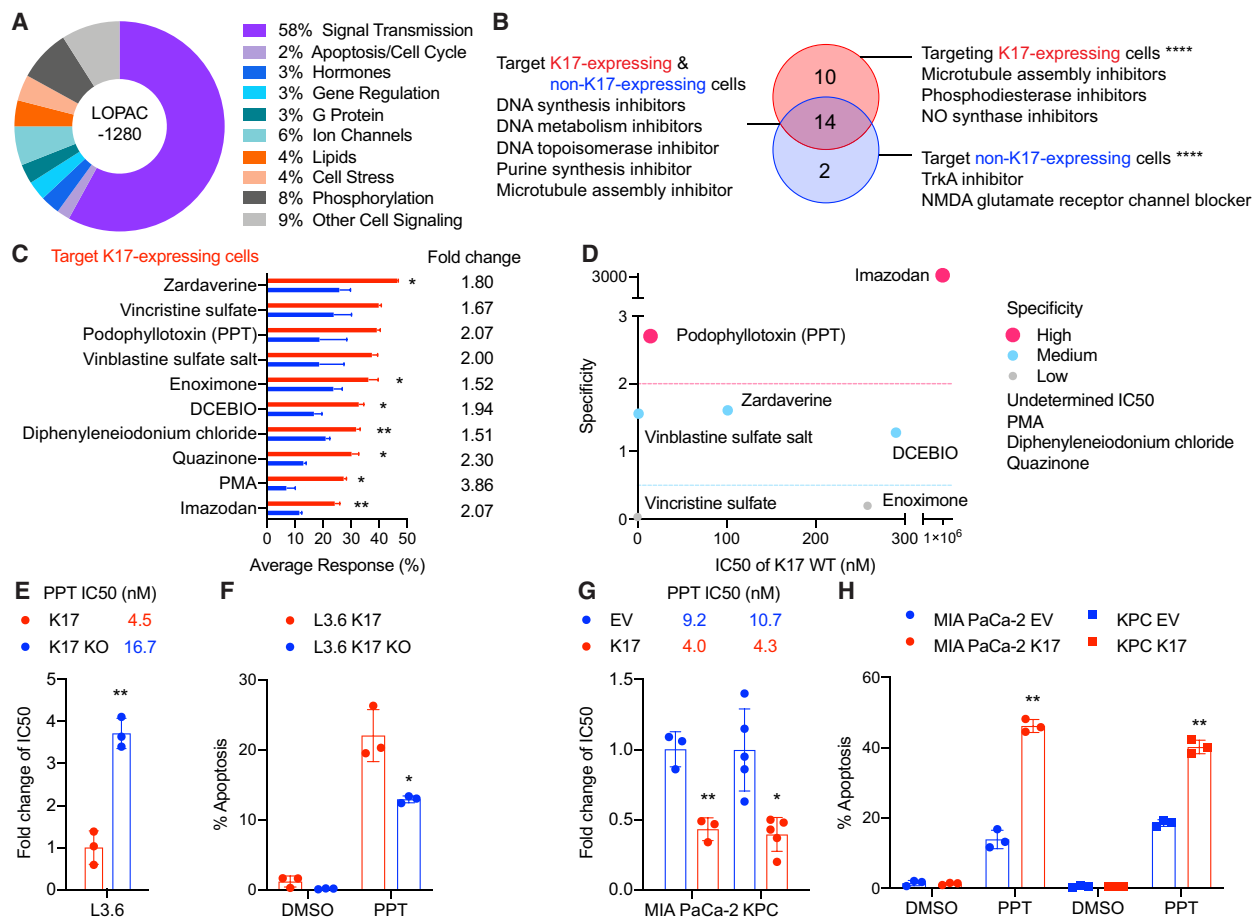


Fig. 4. High-throughput drug screening identifies compounds that specifically target K17-expressing PDAC cells. (A) LOPAC includes 1280 pharmacologically active compounds some of which are marketed drugs and pharmaceutically relevant structures annotated with various biological activities (shown in percent). (B) The primary screen (testing L3.6 K17-expressing cells) and the counterscreen (testing L3.6 K17 KO cells) yielded 26 hits that were organized into three categories based on percent average response rate (at the P -values < 0.0001). (C) Drugs specifically targeting K17-expressing cells are listed. The average response rate and fold change of average response rate between K17-expressing and K17 KO cells are shown (mean \pm SEM). (D) Validation of the 10 drugs that found to be selective for K17-expressing cells. IC50 was determined in K17-expressing and K17 KO cells by CellTiter-Glo[®] assay. The fold change of IC50 was calculated, and the specificity was then determined by the following equation: IC50 of K17 KO cells/IC50 of K17-expressing cells. Specificity: > 2 : high; 0.5 – 2 : medium; < 0.5 : low. (E) Validation of PPT in L3.6 K17 LOF cell line model using WST-1 assay. K17 KO cells show significantly higher IC50 values than K17-expressing cells. IC50 values and fold change of IC50 are shown. (F) L3.6 K17 KO cells showed significantly decreased percent apoptosis than K17-expressing cells under PPT treatment. (G) Validation of PPT in K17 GOF cell line models using WST-1 assay. MIA PaCa-2 and KPC K17 cells showed significantly lower IC50 values than EV cells. IC50 values and fold change of IC50 are shown. (H) MIA PaCa-2 and KPC K17 cells showed significantly increased % apoptosis than EV cells under PPT treatment. Data are shown in mean \pm SD. * $P < 0.5$, ** $P < 0.01$, $n = 3$ – 5 . Student's t -test.

10 compounds fell into two main categories: those that inhibit microtubule assembly (vincristine sulfate, PPT, and vinblastine sulfate salt) and those that inhibit phosphodiesterase activity (zardaverine, enoximone, quazinone, and imazodan). Of note, in this LOPAC screening, three compounds, zardaverine, vincristine sulfate, and PPT, showed the highest response rates among the 10 candidate hits (Fig. 4C and Table 1). To validate the 10 candidates, we performed dose-

dependent treatments to determine the IC50 values in L3.6 cell line model and compounds were further defined as having high, medium, or low specificity for K17-expressing cells (Fig. 4D). By cross-referencing results from these assays to determine selectivity, we found that PPT was the compound with the highest degree of specificity for K17-expressing cells and also required the lowest concentration to inhibit cell viability.

Table 1. Hits identified from the screen and counterscreen, with the cutoff parameter at 23% and 26%, respectively. C, counterscreen; S, screen.

From	Drug name	Description	Average response rate (%)	
			K17	KO
S	Zardaverine	Phosphodiesterase III (PDE III) and phosphodiesterase IV (PDE IV) inhibitor	46.69	26.00
S	Vincristine sulfate	Inhibitor of microtubule assembly	40.08	24.00
S	PPT	Inhibitor of microtubule assembly	39.40	18.99
S	Vinblastine sulfate salt	Inhibitor of microtubule assembly	37.66	18.87
S	Enoximone	Selective phosphodiesterase III (PDE III) inhibitor	36.40	23.92
S	DCEBIO	Increases epithelial chloride secretion through the synergistic activation of a basolateral membrane-located K ⁺ channel (hK1) and an apical membrane Cl ⁻ conductance	32.95	16.96
S	Diphenylethiodonium chloride	Endothelial NO synthase inhibitor	32.02	21.17
S	Quazinone	Phosphodiesterase III (PDE III) inhibitor	30.39	13.23
S	PMA	Activates protein kinase C <i>in vivo</i> and <i>in vitro</i> ; strong NO promoter; promotes expression of iNOS in cultured hepatocytes; T-lymphocyte activator	27.61	7.15
S	Imazodan	Selective phosphodiesterase II (PDE II) inhibitor	24.40	11.80
S/C	Ouabain	Blocks movement of the H5 and H6 transmembrane domains of Na ⁺ -K ⁺ ATPases	83.34	75.43
S/C	Camptothecin	DNA topoisomerase I inhibitor	69.58	70.77
S/C	Mitoxantrone	DNA synthesis inhibitor	65.63	71.47
S/C	Emetine dihydrochloride hydrate	Apoptosis inducer; RNA-protein translation inhibitor	58.26	45.53
S/C	Brefeldin A	Fungal metabolite that disrupts the structure and function of the Golgi apparatus	57.72	45.18
S/C	Dihydroouabain	Na ⁺ -K ⁺ pump inhibitor	48.59	37.74
S/C	Thapsigargin	Potent, cell-permeable, IP ₃ -independent intracellular calcium releaser	48.59	37.74
S/C	Nocodazole	Disrupts microtubules by binding to beta-tubulin	46.91	36.98
S/C	Azathioprine	Purine analog; purine synthesis inhibitor; immunosuppressant	44.85	52.99
S/C	Cytarabine hydrochloride	Selective inhibitor of DNA synthesis	33.90	36.36
S/C	Ancitabine hydrochloride	Antineoplastic DNA metabolism inhibitor	32.32	30.87
S/C	Tyrphostin AG 1478	Selective inhibitor of epidermal growth factor receptor protein	30.67	32.03
S/C	PTX	Antitumor agent; promotes assembly of microtubules and inhibits tubulin disassembly process	29.63	41.74
S/C	3-Amino-1-propanesulfonic acid sodium	GABA-A receptor agonist	26.07	40.16
C	N-(3,3-Diphenylpropyl) glycinamide	NMDA glutamate receptor open-channel blocker.	5.59	28.87
C	Tyrphostin AG 879	Tyrosine kinase nerve growth factor receptor (TrkA) inhibitor; inhibits 140 trk protooncogene and HER-2	6.28	28.94

Podophyllotoxin is known to block cell division by destabilizing microtubule activity through binding tubulin [27]. To confirm the specificity of PPT in inhibiting K17-expressing PDAC cells, we performed an independent validation in additional K17-manipulated cell line models using the WST-1 cell viability assay. In L3.6 (Fig. 4E), MIA PaCa-2, and KPC (Fig. 4G) cell line models, PPT consistently demonstrated at least twofold differences in the IC₅₀ values of K17-expressing cells vs non-K17-expressing cells. Therefore, less than half of the dosage of PPT was required to exert the same inhibitory effect in K17-positive cells, as compared to K17-negative cells. In

addition, under PPT treatment, K17-positive cells showed significantly increased apoptosis compared to K17-negative cells in L3.6 (Fig. 4F), MIA PaCa-2, and KPC (Fig. 4H) cells. These data suggest that PPT induced more apoptotic cell death in K17-expressing cells.

Compared with additional validation experiments of zardaverine from the same category (Fig. S1A,B), however, PTT was the only compound that consistently targeted K17-expressing cells across all models. Thus, through multiple independent validations of several cell lines, we demonstrated that PPT is selectively effective in targeting K17-expressing PDAC cells.

Lastly, we validated additional compounds in the other two categories from the initial single-dose screen with higher response rates. In the category of compounds that show similar efficacy in both K17-expressing and K17 KO cells, mitoxantrone was selected for further studies because it shares a similar mechanism of action to current standard-of-care chemotherapeutic agents (DNA synthesis inhibitor) for PDAC [28]. Validation experiments showed that mitoxantrone had similar sensitivity in K17-expressing and non-K17-expressing cells in all three cell line models (Fig. S1D, E). In addition, tyrphostin AG 879, the drug targeting the K17 KO cells with the highest average response, was chosen for further studies (Fig. S1H–J). We validated that this drug was much more sensitive in L3.6 K17 KO cells (Fig. S1I); however, it was highly resistant in MIA PaCa-2 and KPC cells (Fig. S1J), potentially due to phenotypic differences between cell line models and off-target effects. These verify results from the screen in L3.6 cell line model (Fig. S1C) and suggest that validation experiments of a high-throughput drug screen are necessary to confirm the on-target effect.

In summary, using an unbiased single-dose high-throughput drug screen followed by dose-dependent treatment experiments, we identified and validated PPT as a potential drug to target K17-expressing PDAC cells.

3.4. Targeting microtubule assembly rather than microtubule disassembly is a therapeutic vulnerability in K17-expressing pancreatic cancers

To evaluate whether PPT might enhance Gem-mediated cytotoxicity and determine whether the combined effect is synergistic, additive, or antagonistic, we measured cell viability by treating with increasing doses of the combination of Gem and PPT at fixed ratios, as following: 1 : 1 in L3.6 cells and 37.5 : 1 in MIA PaCa-2 and KPC cells, based on their IC₅₀ values of Gem and PPT, according to established protocols [29]. We found that K17-expressing cells had significantly lower cell viability under the same doses compared with non-K17-expressing cells (Fig. S2A–C). In addition, the IC₅₀ of the combination of Gem and PPT was lower in K17-expressing cells compared to isogenic cells lacking K17 expression. We computed the CI [25] to determine the interaction of Gem and PPT in PDAC cells. Along with increasing effective doses from 50% to 97% of cell viability, the combination of Gem and PPT demonstrated a strongly synergistic interaction as shown by CI values lower than 0.9 in

L3.6 K17-expressing cells, and there was an additive (effective dose at 50–75%) to antagonistic (effective dose at 90–97%) effect in L3.6 K17 KO cells (Fig. 5A). In MIA PaCa-2 cell line model, cotreatment showed an additive (effective dose at 50%) to antagonistic effect (effective doses at 75–97%) in K17-expressing (K17) cells and an antagonistic effect in non-K17-expressing (EV) cells (Fig. 5B). In KPC cells, a strongly synergistic effect was found in KPC K17 cells (CI < 0.5) while an antagonistic effect was observed in KPC EV cells (Fig. 5C). In summary, we demonstrated that PPT in combination with Gem was synergistic or additive in K17-expressing cells but that these drugs had antagonistic effects in non-K17-expressing cells.

To validate the *in vitro* results, we used the orthotopic xenograft model to determine the anticancer effect of PPT alone and Gem in combination with PPT in K17-positive and K17-negative tumors. At day 14 post-treatments, in K17-negative tumors (KPC EV), treatments of PPT alone or the combination did not affect tumor growth (Fig. 6A). Importantly, in K17-positive tumors (KPC K17), treatments of PPT alone or the combination significantly inhibited tumor growth (Fig. 6B, the tumor sizes reduced to half of the size of controls). In addition, PPT treatment alone significantly extended survival (HR = 0.3944, Log-rank $P = 0.034$) only in mice bearing K17-expressing tumors but not those with non-K17-expressing tumors (Fig. 6C,D, green curves). These results strengthen our *in vitro* findings that K17-expressing PDAC cells were more sensitive to PPT. Interestingly, the combination of Gem and PPT significantly extended survival in mice with both K17-positive and K17-negative tumors (Fig. 6C,D, orange curves), compared with saline controls or PPT treatment alone. However, the highest survival advantage was observed in mice bearing K17-expressing tumors (median survival in days: EV = 32.5 and K17 = 44.5). During the treatment period, the mice tolerated all the treatments without significant body weight differences (Fig. S3A,B). Overall, these data show that when PDAC tumors express K17, they are more sensitive to the treatments of PPT alone or the combination of Gem and PPT.

Currently, Gem is combined with PTX (taxol, PTX), a compound that stabilizes microtubules and protects it from disassembly [30] as a standard-of-care therapeutic regimen for PDAC [7]. Given that we identified PPT, a compound that destabilizes microtubules [27], to be synergistic when combined with Gem in K17-expressing PDACs, we set out to determine whether the synergistic effect of Gem in combination with a microtubule inhibitor depends on a

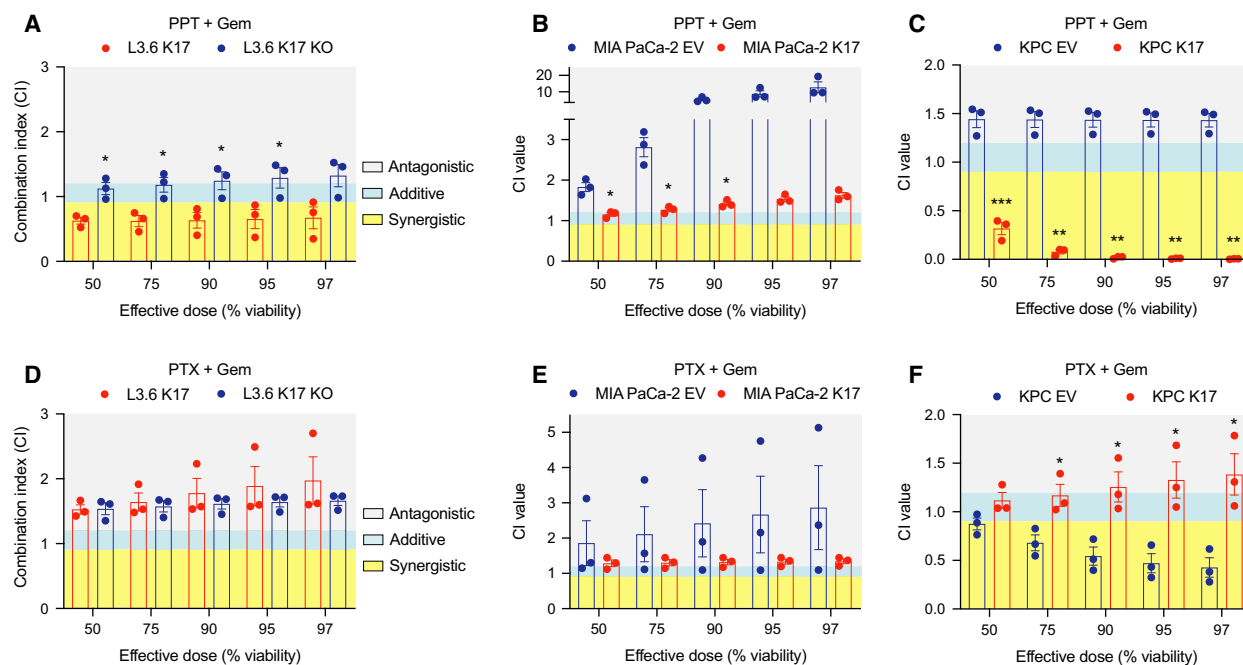


Fig. 5. When combined with Gem, PPT, but not PTX, shows synergistic effects in inhibiting the viability of K17-expressing PDAC cells. (A–C) The combination effects of PPT and Gem in L3.6 (A), MIA PaCa-2 (B), and KPC (C) cell line models were determined by calculating the CI values at effective dose at 50, 75, 90, 95, and 97 percent of cell viability. (D, E) The combination effects of PTX and Gem in L3.6 (D), MIA PaCa-2 (E), and KPC (F) cell line models were determined by calculating the CI values at effective dose at 50, 75, 90, 95, and 97 percent of cell viability. CI < 0.9 indicates a synergistic effect. CI = 0.9–1.2 indicates an additive effect. CI > 1.2 indicates an antagonistic effect. Data are shown in mean \pm SEM. * P < 0.05, ** P < 0.01, *** P < 0.001, n = 3. Student's t -test.

specific mechanism of action of PPT and/or PTX. First, we tested the IC₅₀ values of PTX and found that they were similar in K17-positive vs K17-negative cells in L3.6 and KPC cell lines (Fig. S1F,G) and the IC₅₀ was lower in K17 cells than in EV cells in MIA PaCa-2 cell line model (Fig. S1G). Second, we tested the combination of PTX and Gem, using the same experimental setup of testing PPT combined with Gem. We found no obvious differences in the dose–response curves of the combination in K17-positive and K17-negative cells (Fig. S2D–F). Surprisingly, we found that PTX and Gem tended to have antagonistic effects in K17-expressing cells across isogenic model systems (Fig. 5D,F), while it only showed synergistic effects in KPC cells lacking K17 expression (Fig. 5F).

Together, we found that K17 expression sensitizes cells to PPT in combination with Gem; however, these effects are adverse when Gem is combined with PTX in the same cells, suggesting that the mode of action of microtubule dynamic inhibitors may have a direct and/or indirect effect on K17 intermediate filament dynamic or function. Future studies, however, are needed to test this hypothesis.

4. Discussion

Here, we identify that expression of K17 in PDACs correlates and causes resistance to Gem treatment, while it sensitizes cells to an US Food and Drug Administration (FDA)-approved compound that causes microtubule disassembly, identified by high-throughput screen and downstream validation assays. In addition, we found that the combination of Gem and this microtubule inhibitor synergizes to specifically target K17-expressing PDACs. This study is important as it reports a biomarker-based novel combination therapy that can be further tested in preclinical and clinical settings to target the most lethal molecular subtype of pancreatic cancer.

The report of the PDAC molecular subtypes was a key milestone for the advancement in understanding this highly lethal disease, opening three crucial research areas: (a) development of clinical tests to subtype patients at the time of diagnosis; (b) selection of the best standard of care (Gem/nab-PTX or FOLFIRINOX) for each molecular subtype; and (c) identification of targeted therapies, based on PDAC subtypes.

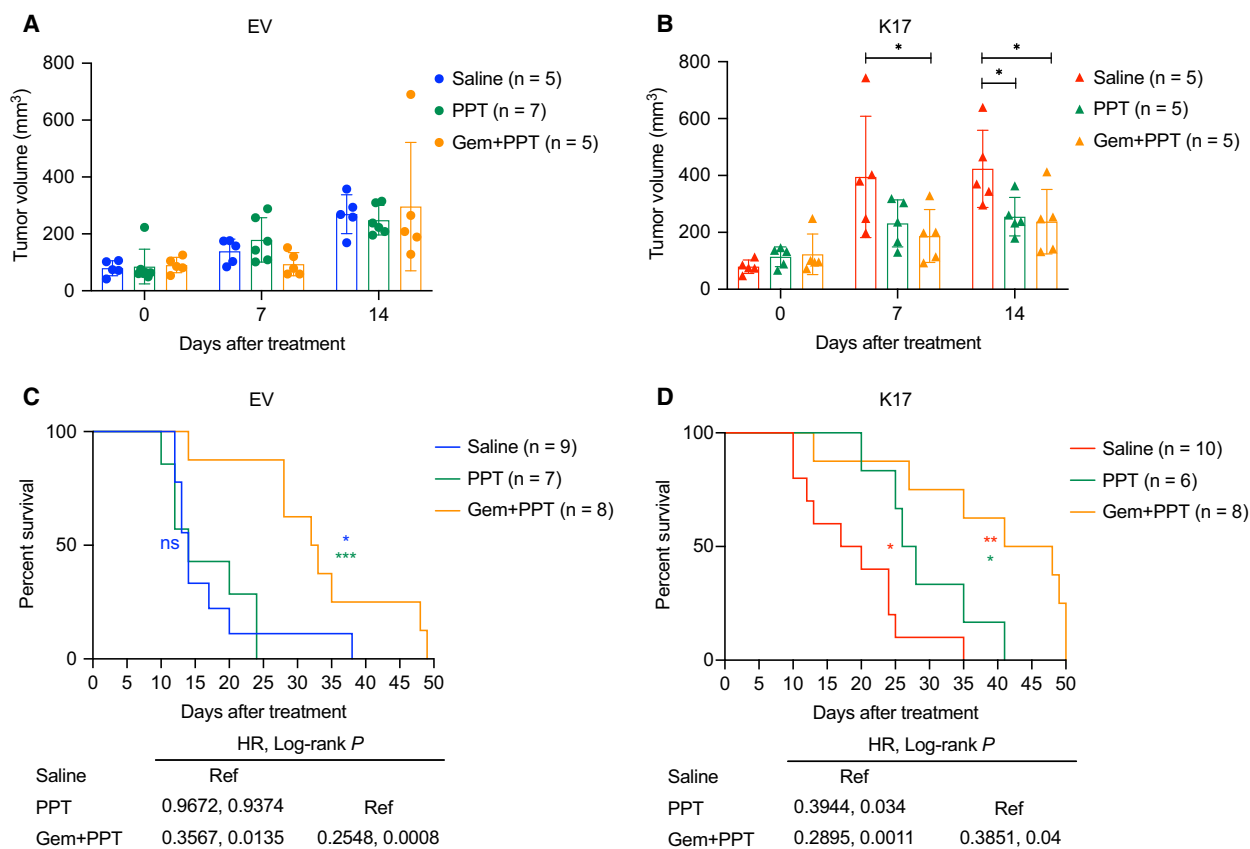


Fig. 6. The treatment of PPT alone or the combination of Gem and PPT shows higher anticancer effects in K17-expressing PDACs. (A) With PPT or combination treatments, tumor volumes of KPC non-K17-expressing tumors (EV) were not decreased. (B) With PPT or combination treatments, tumor volumes of KPC K17-expressing tumors (K17) were significantly decreased. (C) PPT treatment did not extend the survival of animals bearing non-K17-expressing (EV) tumors. Gem combined with PPT significantly extend the survival of animals bearing non-K17-expressing (EV) tumors. (D) Treatments of PPT alone and Gem combined with PPT significantly extended the survival of animals bearing K17-expressing (K17) tumors. Data are shown in mean \pm SD. * $P < 0.5$, ** $P < 0.01$, *** $P < 0.001$ $n = 5-10$. Student's *t*-test.

It is critically important to develop clinical tests to subtype PDAC patients at the time of diagnosis, to provide the most appropriate therapy. We recently reported that K17 mRNA, a hallmark biomarker of the most lethal molecular subtype of PDAC, is as accurate as molecular subtyping to identify the PDAC patient population with the worst prognosis [17]. Moreover, K17 protein, as detected by immunohistochemistry (IHC), provides better prognostic value than mRNA. Importantly, we have established a protocol for K17 IHC that can be used both in research laboratory and in clinical laboratory diagnostic settings. As the only reported basal-like gene that provides both prognostic and predictive values, further studies are required to validate K17's predictive value at the protein level using IHC.

To date, there are no predictive biomarkers to inform PDAC response to either Gem/nab-PTX or

FOLFIRINOX regimens [31,32], to enhance therapeutic efficacy, or to prevent adverse effects based on the molecular characteristics of the tumors. Based on our findings, K17 may be a candidate predictive biomarker for response to Gem/nab-PTX. Importantly, the COMPASS trial findings show that basal-like PDACs tended to be more resistant to the FOLFIRINOX chemotherapy [15,33]. Our data also suggest that K17 promotes resistance to 5-FU, a main agent in FOLFIRINOX. As such, it is important to determine whether K17 is a predictive marker of FOLFIRINOX in PDAC. It has been shown that basal-like cells are more sensitive to Gem compared to classical cells in PDAC cell lines [13]. Here, we demonstrated that K17, a basal-like signature gene, promotes chemoresistance in PDAC cell lines. This discrepancy may due to the fact that there is not a 1 : 1 correlation between K17 status and molecular subtype in PDAC cell lines. In

addition, the molecular subtypes are defined by a panel of genes and all the signature genes may interrelate through their different roles in cellular responses to treatment. To our knowledge, K17 is the only gene expressed in the most lethal basal-like subtype of PDAC that actively promotes chemoresistance to Gem and 5-FU and thus may represent a potential clinical target for personalized treatment.

With the goal of identifying novel targeted therapies using existing FDA-approved compounds that can be repurposed and fast-tracked for the treatment of the patients with K17-expressing PDACs, we performed a high-throughput drug screen using the LOPAC assay. Although previous LOPAC screens had been applied to PDAC cell lines [34], to date, these screens have not been evaluated in the context of PDAC molecular subtypes and in combination with current chemotherapeutic agents. Through validation studies in three different K17 LOF and GOF PDAC cell line models, we report that PPT was consistently found to preferentially target K17-expressing cells. Our findings suggest that microtubule assembly inhibitors may be potentially effective drugs for treating K17-expressing PDACs. These observations are novel because the combination of PPT and Gem as a potential regimen for cancer therapy has not been previously reported. Furthermore, we also found that PPT was the most effective agent to target K17-expressing PDAC cells and that it synergizes in combination with Gem. Surprisingly, these effects were not recapitulated when combining Gem with PTX. This suggests that the current standard-of-care therapy may be replaced by a more effective and synergistic combination: Gem and PPT. Although beyond the scope of this study, future studies should address the mechanistic basis regarding how K17 expression sensitizes PDAC cells to PPT treatment.

Importantly, compared to other microtubule inhibitors from our LOPAC screen (such as PTX, vincristine sulfate, and vinblastine sulfate salt), PPT showed the highest specificity in inhibiting K17-expressing PDACs. In a previous study, PPT was shown to significantly inhibit the growth of lung tumor cells and using *in vitro* and *in vivo* models was cytotoxic in several human cancer cell lines [35–38]. Although PPT is currently only used for treatment of HPV-mediated cutaneous lesions, its semisynthetic compounds, etoposide and teniposide, are widely used for cancer therapy in the clinic. A phase II trial previously showed that Gem combined with etoposide exhibited a response rate similar to published trials using Gem-based chemotherapies [39]. Despite extensive interest in utilizing PPT and its derivatives for cancer therapy, very

few of these agents have reached clinical practice, in part due to toxicity and solubility [40–42]. More selective PPT derivatives based on modified structures may enhance effective responses in K17-expressing PDACs. Future studies of testing the specificity of etoposide and teniposide, alone and in combination with Gem in K17-expressing PDACs, are needed.

In summary, we discovered a novel therapeutic vulnerability of K17-expressing PDACs and identified a compound that, when combined with Gem, may enhance tumor response, compared to the current standard of care with Gem/nab-PTX.

5. Conclusions

The identification of biomarker-driven novel therapies is a critical priority for improving survival of PDAC patients. K17 is a novel target for development of a biomarker-based personalized treatment for the most aggressive form of PDAC [43]. We demonstrated that beyond its predictive value, K17 drives chemoresistance to Gem and 5-FU. Through an unbiased drug screen, we discovered that PPT showed at least two-fold higher sensitivity in K17-positive PDAC cells. Surprisingly, we found that small molecules that inhibit microtubule assembly (PPT) rather than microtubule disassembly (PTX) specifically target K17 PDACs, uncovering a novel therapeutic vulnerability of the most aggressive molecular subtype of PDAC. These studies serve as scientific premise to further launch preclinical testing of this novel combination therapy that can guide optimal therapeutic management, which is driven by data related to the molecular composition and biomarker expression in PDACs.

Acknowledgements

The authors thank Dr. Peter Bailey and the APGI for RNA-Seq data, Dr. Coulombe Pierre (University of Michigan) for providing the K17 antibody, Dr. Wei-Xing Zong (Rutgers University) for L3.6 cells, Dr. Gerardo Mackenzie (University of California at San Diego) for KPC cells, and all members of our laboratory for critical review of the manuscript. This work was supported by the 2018 Pancreatic Cancer Action Network Translational Research Grant, 18-65-SHRO (KRS), National Cancer Institute K99-R00 Grant, CA226342-01 (LFE-H), Pancreatic Cancer Action Network—AACR Pathway to Leadership Grant, 17-70-25-ESCO (LFE-H), National Pancreas Foundation Grants (LFE-H and CVL), Hirshberg Foundation (LFE-H), and National Institutes of Health Loan Repayment Programs (CVL).

Conflict of interest

LFE-H and KRS are consultants for KDx Diagnostics Inc. and OncoGenesis Inc.

Author contributions

C-HP, TS, LFE-H, and KRS designed the research. SB, DKC, and AVB performed patient data analyses. C-HP, CVL, RRK, and JDKB generated cell line models. YO and BS performed drug screening. C-HP, YO, and MW performed validation experiments and analyzed the data. C-HP, CVL, and MTG performed animal studies. LS and TS supervised the high-throughput compound screening study. LFE-H and KRS supervised the patient data analyses, and *in vitro* and *in vivo* validation studies. C-HP and MW wrote the manuscript. YO, CVL, TS, LFE-H, and KRS edited and revised the manuscript. All authors have read and approved the final manuscript.

References

- Siegel RL, Miller KD & Jemal A (2019) Cancer statistics, 2019. *CA Cancer J Clin* **69**, 7–34.
- Kleeff J, Korc M, Apte M, La Vecchia C, Johnson CD, Biankin AV, Neale RE, Tempero M, Tuveson DA, Hruban RH *et al.* (2016) Pancreatic cancer. *Nat Rev Dis Primers* **2**, 16022.
- Gnanamony M & Gondi CS (2017) Chemoresistance in pancreatic cancer: emerging concepts. *Oncol Lett* **13**, 2507–2513.
- Zeng S, Pottler M, Lan B, Grutzmann R, Pilarsky C & Yang H (2019) Chemoresistance in pancreatic cancer. *Int J Mol Sci* **20**.
- Kommalapati A, Tella SH, Goyal G, Ma WW & Mahipal A (2018) Contemporary management of localized resectable pancreatic cancer. *Cancers (Basel)* **10**.
- Giuliani F, Di Maio M, Colucci G & Perrone F (2012) Conventional chemotherapy of advanced pancreatic cancer. *Curr Drug Targets* **13**, 795–801.
- Von Hoff DD, Ervin T, Arena FP, Chiorean EG, Infante J, Moore M, Seay T, Tjulandin SA, Ma WW, Saleh MN *et al.* (2013) Increased survival in pancreatic cancer with nab-paclitaxel plus gemcitabine. *N Engl J Med* **369**, 1691–1703.
- Conroy T, Desseigne F, Ychou M, Bouche O, Guimbaud R, Becouarn Y, Adenis A, Raoul JL, Gourgou-Bourgade S, de la Fouchardiere C *et al.* (2011) FOLFIRINOX versus gemcitabine for metastatic pancreatic cancer. *N Engl J Med* **364**, 1817–1825.
- McGuigan A, Kelly P, Turkington RC, Jones C, Coleman HG & McCain RS (2018) Pancreatic cancer: a review of clinical diagnosis, epidemiology, treatment and outcomes. *World J Gastroenterol* **24**, 4846–4861.
- Chand S, O'Hayer K, Blanco FF, Winter JM & Brody JR (2016) The landscape of pancreatic cancer therapeutic resistance mechanisms. *Int J Biol Sci* **12**, 273–282.
- Bailey P, Chang DK, Nones K, Johns AL, Patch AM, Gingras MC, Miller DK, Christ AN, Bruxner TJ, Quinn MC *et al.* (2016) Genomic analyses identify molecular subtypes of pancreatic cancer. *Nature* **531**, 47–52.
- Collisson EA, Bailey P, Chang DK & Biankin AV (2019) Molecular subtypes of pancreatic cancer. *Nat Rev Gastroenterol Hepatol* **16**, 207–220.
- Collisson EA, Sadanandam A, Olson P, Gibb WJ, Truitt M, Gu S, Cooc J, Weinkle J, Kim GE, Jakkula L *et al.* (2011) Subtypes of pancreatic ductal adenocarcinoma and their differing responses to therapy. *Nat Med* **17**, 500–503.
- Moffitt RA, Marayati R, Flate EL, Volmar KE, Loeza SG, Hoadley KA, Rashid NU, Williams LA, Eaton SC, Chung AH *et al.* (2015) Virtual microdissection identifies distinct tumor- and stroma-specific subtypes of pancreatic ductal adenocarcinoma. *Nat Genet* **47**, 1168–1178.
- Aung KL, Fischer SE, Denroche RE, Jang GH, Dodd A, Creighton S, Southwood B, Liang SB, Chadwick D, Zhang A *et al.* (2018) Genomics-driven precision medicine for advanced pancreatic cancer: early results from the COMPASS Trial. *Clin Cancer Res* **24**, 1344–1354.
- Lipner MB & Yeh JJ (2018) Sequencing pancreatic juice: squeezing the most out of surveillance. *Clin Cancer Res* **24**, 2713–2715.
- Roa-Peña L, Leiton CV, Babu S, Pan CH, Vanner EA, Akalin A, Bandovic J, Moffitt RA, Shroyer KR & Escobar-Hoyos LF (2019) Keratin 17 identifies the most lethal molecular subtype of pancreatic cancer. *Sci Rep* **9**.
- Ballman KV (2015) Biomarker: predictive or prognostic? *J Clin Oncol* **33**, 3968–3971.
- Rajapakse VN, Luna A, Yamada M, Loman L, Varma S, Sunshine M, Iorio F, Sousa FG, Elloumi F, Aladjem MI *et al.* (2018) CellMinerCDB for integrative cross-database genomics and pharmacogenomics analyses of cancer cell lines. *iScience* **10**, 247–264.
- Bruns CJ, Harbison MT, Kuniyasu H, Eue I & Fidler IJ (1999) *In vivo* selection and characterization of metastatic variants from human pancreatic adenocarcinoma by using orthotopic implantation in nude mice. *Neoplasia* **1**, 50–62.
- Depianto D, Kerns ML, Dlugosz AA & Coulombe PA (2010) Keratin 17 promotes epithelial proliferation and tumor growth by polarizing the immune response in skin. *Nat Genet* **42**, 910–914.

- 22 Hobbs RP, DePianto DJ, Jacob JT, Han MC, Chung BM, Batazzi AS, Poll BG, Guo Y, Han J, Ong S *et al.* (2015) Keratin-dependent regulation of Aire and gene expression in skin tumor keratinocytes. *Nat Genet* **47**, 933–938.
- 23 McGowan KM & Coulombe PA (1998) Onset of keratin 17 expression coincides with the definition of major epithelial lineages during skin development. *J Cell Biol* **143**, 469–486.
- 24 Pan CH, Chang YF, Lee MS, Wen BC, Ko JC, Liang SK & Liang MC (2016) Vorinostat enhances the cisplatin-mediated anticancer effects in small cell lung cancer cells. *BMC Cancer* **16**, 857.
- 25 Chou TC (2010) Drug combination studies and their synergy quantification using the Chou-Talalay method. *Cancer Res* **70**, 440–446.
- 26 Escobar-Hoyos LF, Shah R, Roa-Pena L, Vanner EA, Najafian N, Banach A, Nielsen E, Al-Khalil R, Akalin A, Talmage D *et al.* (2015) Keratin-17 promotes p27KIP1 nuclear export and degradation and offers potential prognostic utility. *Cancer Res* **75**, 3650–3662.
- 27 Gordaliza M, Castro MA, del Corral JM & Feliciano AS (2000) Antitumor properties of podophyllotoxin and related compounds. *Curr Pharm Des* **6**, 1811–1839.
- 28 Flores JP, Diasio RB & Saif MW (2017) Drug metabolism and pancreatic cancer. *Ann Gastroenterol* **30**, 54–61.
- 29 Tallarida RJ (2011) Quantitative methods for assessing drug synergism. *Genes Cancer* **2**, 1003–1008.
- 30 Weaver BA (2014) How Taxol/paclitaxel kills cancer cells. *Mol Biol Cell* **25**, 2677–2681.
- 31 Hasan S, Jacob R, Manne U & Paluri R (2019) Advances in pancreatic cancer biomarkers. *Oncol Rev* **13**, 410.
- 32 Le N, Sund M, Vinci A & Gems collaborating group of Pancreas (2016) Prognostic and predictive markers in pancreatic adenocarcinoma. *Dig Liver Dis* **48**, 223–230.
- 33 O’Kane GM, Grunwald BT, Jang GH, Masoomian MP, Picardo S, Grant RC, Denroche RE, Zhang A, Wang Y, Lam B *et al.* (2020) GATA6 expression distinguishes classical and basal-like subtypes in advanced pancreatic cancer. *Clin Cancer Res* **31**.
- 34 Kim I, Choi YS, Song JH, Choi EA, Park S, Lee EJ, Rhee JK, Kim SC & Chang S (2018) A drug-repositioning screen for primary pancreatic ductal adenocarcinoma cells identifies 6-thioguanine as an effective therapeutic agent for TPMT-low cancer cells. *Mol Oncol* **12**, 1526–1539.
- 35 Choi JY, Hong WG, Cho JH, Kim EM, Kim J, Jung CH, Hwang SG, Um HD & Park JK (2015) Podophyllotoxin acetate triggers anticancer effects against non-small cell lung cancer cells by promoting cell death via cell cycle arrest, ER stress and autophagy. *Int J Oncol* **47**, 1257–1265.
- 36 Liu JF, Sang CY, Xu XH, Zhang LL, Yang X, Hui L, Zhang JB & Chen SW (2013) Synthesis and cytotoxic activity on human cancer cells of carbamate derivatives of 4beta-(1,2,3-triazol-1-yl)podophyllotoxin. *Eur J Med Chem* **64**, 621–628.
- 37 Wrasidlo W, Gaedicke G, Guy RK, Renaud J, Pitsinos E, Nicolaou KC, Reisfeld RA & Lode HN (2002) A novel 2’-(N-methylpyridinium acetate) prodrug of paclitaxel induces superior antitumor responses in preclinical cancer models. *Bioconjug Chem* **13**, 1093–1099.
- 38 Zi CT, Gao YS, Yang L, Feng SY, Huang Y, Sun L, Jin Y, Xu FQ, Dong FW, Li Y *et al.* (2019) Design, synthesis, and biological evaluation of novel biotinylated podophyllotoxin derivatives as potential antitumor agents. *Front Chem* **7**, 434.
- 39 Melnik MK, Webb CP, Richardson PJ, Luttenton CR, Campbell AD, Monroe TJ, O’Rourke TJ, Yost KJ, Szczepanek CM, Bassett MR *et al.* (2010) Phase II trial to evaluate gemcitabine and etoposide for locally advanced or metastatic pancreatic cancer. *Mol Cancer Ther* **9**, 2423–2429.
- 40 Ardalani H, Avan A & Ghayour-Mobarhan M (2017) Podophyllotoxin: a novel potential natural anticancer agent. *Avicenna J Phytomed* **7**, 285–294.
- 41 Newman DJ, Cragg GM and Kingston DGI (2015) Natural products as pharmaceuticals and sources for lead structures. In *The Practice of Medicinal Chemistry*, 4th edn (Wermuth CG, Aldous D, Raboisson P & Rognan D, eds), pp. 102–131. Academic Press, San Diego, CA.
- 42 Theobald RJ (2016) Podophyllotoxin. In *Reference Module in Biomedical Sciences* (Caplan M, ed). Elsevier, Amsterdam, Netherlands.
- 43 Shroyer KR & Escobar Hoyos LF (2015) Keratin 17 as a prognostic marker for pancreatic cancer. United States Patent and Trademark Office, Alexandria, VA.

Supporting information

Additional supporting information may be found online in the Supporting Information section at the end of the article.

Fig. S1. Validation of compounds in other categories. (A, B) Validation of Zardaverine in L3.6 (A) and in MIA PaCa-2 and KPC cell line models (B). IC₅₀ values, fold change of IC₅₀ or cell viability (WST-1 relative index) are shown. (C) Drugs targeting both L3.6 K17 expressing and KO cells from the Screen and the Counterscreen are listed. Fold change of average response rate are shown (mean ± SEM). (D, E) Validation of Mitoxantrone in L3.6 (D) and in MIA PaCa-2 and KPC cell line models (E). IC₅₀ values and fold change of IC₅₀ are shown. (F, G) Validation of

PTX in L3.6 (F) and in MIA PaCa-2 and KPC cell line models (G). IC50 values and fold change of IC50 are shown. (H) Drugs targeting L3.6 K17 KO cells from the Screen and the Counterscreen are listed. Fold change of average response rate are shown (mean \pm SEM). (I, J) Validation of Tyrophostin AG879 in L3.6 (I) and in MIA PaCa-2 and KPC cell line models (J). IC50 values, fold change of IC50 or cell viability (WST-1 relative index) are shown. Data are shown in mean \pm SD. * $P < 0.05$, ** $P < 0.01$, $n = 3-4$. Student's *t*-test.

Fig. S2. K17 expressing cells show lower cell viability than non-K17 expressing cells under treatment of PPT and Gem, but no obvious difference is found in PTX and Gem. (A–C) The dose-response curves of PPT combined with Gem were shown in L3.6 (A), MIA PaCa-2 (B) and KPC (C) cell line models. The predicted IC50 of PPT + gem in each cell line were listed. (D–F) The dose-response curves of PTX combined with Gem were shown in L3.6 (D), MIA PaCa-2 (E) and KPC (F) cell line models. The predicted IC50 of PPT + gem in each cell line were listed. Data are shown in mean \pm SD. * $P < 0.05$, ** $P < 0.01$, *** $P < 0.001$, $n = 3$. Student's *t*-test.

Fig. S3. The mice tolerated all the treatments without significant body weight differences in the study of Gem combined with PPT. (A, B) Body weight of mice in each treatment group was shown in KPC EV (A) and K17 (B) tumors.

Fig. S4. Representative dose response curves of each tested drugs. (A–D) Gem treatment in L3.6 K17 LOF cell line model (A), MIA PaCa-2 (B) and KPC (C) K17 GOF cell line models, and L3.6 K17 Rescue cell line model (D). (E–H) 5-FU treatment in L3.6 K17 LOF cell line model (E), MIA PaCa-2 (F) and KPC (G) K17 GOF cell line models, and L3.6 K17 Rescue cell line model (H). (I–K) PPT treatment in L3.6 K17 LOF cell line model (I), MIA PaCa-2 (J) and KPC (K) K17 GOF cell line models. (L–N) Zardaverine treatment in L3.6 K17 LOF cell line model (L), MIA PaCa-2 (M) and KPC (N) K17 GOF cell line models. (O–Q) Mitoxantrone treatment in L3.6 K17 LOF cell line model (O), MIA PaCa-2 (P) and KPC (Q) K17 GOF cell line models. (R–T) PTX treatment in L3.6 K17 LOF cell line model (R), MIA PaCa-2 (S) and KPC (T) K17 GOF cell line models. (U–W) Tyrophostin AG879 treatment in L3.6 K17 LOF cell line model (U), MIA PaCa-2 (V) and KPC (W) K17 GOF cell line models. Data was shown in mean \pm SD. * $P < 0.5$, ** $P < 0.01$, *** $P < 0.001$, $n = 3$. Student's *t*-test.

Fig. S4. Representative dose response curves of each tested drugs.

Table S1. Data used to determine the correlation of K17 expression and Gem sensitivity.

Table S2. Data used to determine the correlation of K17 expression and 5-FU sensitivity.